JACS
JOURNAL OF THE AMERICAN CHEMICAL SOCIETY
Article
pubs.acs.org/JACS

The Role of Stable α-Synuclein Oligomers in the Molecular Events Underlying Amyloid Formation

Nikolai Lorenzen,[†,⊥] Søren Bang Nielsen,[†,#] Alexander K. Buell,[‡] Jørn Døvling Kaspersen,[§] Paolo Arosio,[‡] Brian Stougaard Vad,[†] Wojciech Paslawski,[†] Gunna Christiansen,[∥] Zuzana Valnickova-Hansen,[†] Maria Andreasen,[†] Jan J. Enghild,[†] Jan Skov Pedersen,[§] Christopher M. Dobson,[‡] Tuomas P. J. Knowles,[‡] and Daniel Erik Otzen*[,†]

[†]Department of Molecular Biology, Center for Insoluble Protein Structures (inSPIN) and [§]Department of Chemistry, Interdisciplinary Nanoscience Center (iNANO), Aarhus University, Gustav Wieds Vej 14, 8000 Aarhus C, Denmark

[‡]Department of Chemistry, University of Cambridge, Lensfield Road, CB2 1EW, Cambridge United Kingdom

[∥]Department of Biomedicine-Medical Microbiology and Immunology, Aarhus University, 8000 Aarhus C, Denmark

Supporting Information

ABSTRACT: Studies of proteins' formation of amyloid fibrils have revealed that potentially cytotoxic oligomers frequently accumulate during fibril formation. An important question in the context of mechanistic studies of this process is whether or not oligomers are intermediates in the process of amyloid fibril formation, either as precursors of fibrils or as species involved in the fibril elongation process or instead if they are associated with an aggregation process that is distinct from that generating mature fibrils. Here we describe and characterize in detail two well-defined oligomeric species formed by the protein α-synuclein (αSN), whose aggregation is strongly implicated in the development of Parkinson's disease (PD). The two types of oligomers are both formed under conditions where amyloid fibril formation is observed but differ in molecular weight by an order of magnitude. Both possess a degree of β-sheet structure that is intermediate between that of the disordered monomer and the fully structured amyloid fibrils, and both have the capacity to permeabilize vesicles *in vitro*. The smaller oligomers, estimated to contain ∼30 monomers, are more numerous under the conditions used here than the larger ones, and small-angle X-ray scattering data suggest that they are ellipsoidal with a high degree of flexibility at the interface with solvent. This oligomer population is unable to elongate fibrils and indeed results in an inhibition of the kinetics of amyloid formation in a concentration-dependent manner.

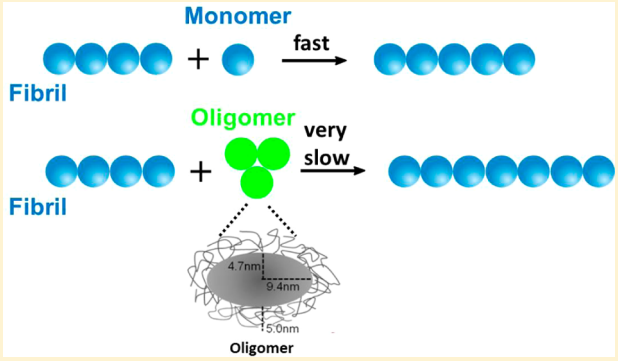

INTRODUCTION

It is increasingly well accepted that soluble oligomers of proteins associated with amyloid formation are the most important toxic species in a range of neurodegenerative disorders such as Parkinson's disease (PD)[1−4] and Alzheimer's disease (AD).[5−10] There is good evidence that these oligomers possess, among other properties, the ability to disrupt membrane functions and thereby have the ability to induce neuronal damage.[2,11,12] Oligomers are often observed in coexistence with amyloid fibrils,[13] but many aspects of the relationship between oligomers and the mechanism of amyloid fibril assembly are not yet understood. In some cases, oligomers appear to be direct building blocks of amyloid fibrils,[14,15] but there are also examples of fibril systems where no significant quantities of oligomers are observed;[16−21] in other cases, the oligomeric species under study have been shown not to be direct precursors of fibrils.[22−26] There are also examples of different assembly processes in given protein systems leading to different types of fibril morphology and structure.[27−29]

Recent advances in modern structural techniques have led to significant increases in our knowledge of the structures of amyloid fibrils, although such information is still limited. Thus, a range of techniques, notably X-ray diffraction of microcrystals,[30] solid-state nuclear magnetic resonance spectroscopy (NMR), and cryo-electron microscopy have provided structural information at different levels of resolution of a series of amyloidogenic peptides and proteins.[31−35] Structural data on oligomers are, however, even sparser due to the transient nature and inherent polydispersity of such species,[36,37] although such problems have been addressed by methods such as photochemical cross-linking[38] and protein engineering.[39]

It is of great importance to understand the role of αSN oligomers in the aggregation process, not least because αSN is a highly validated drug discovery target for PD.[40−43] Here we analyze the role of well-defined αSN oligomers which

Received: November 13, 2013
Published: February 16, 2014

   dx.doi.org/10.1021/ja411577t | J. Am. Chem. Soc. 2014, 136, 3859−3868

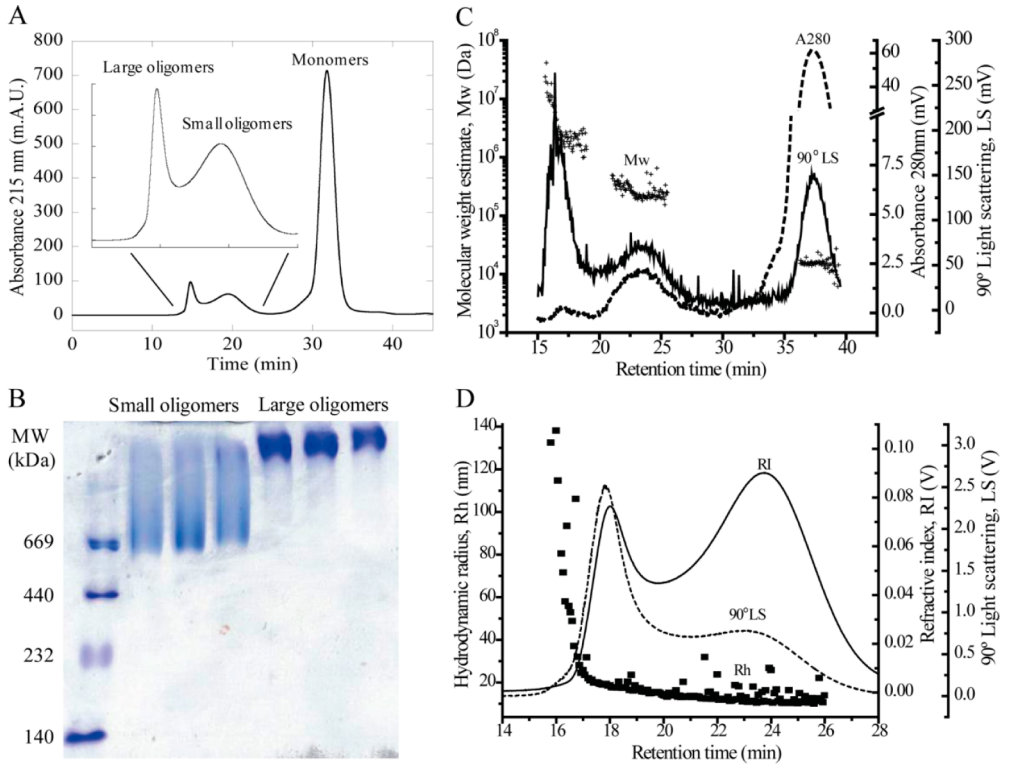

Figure 1. Analysis of the size distribution, molecular weights and hydrodynamic radii of the oligomer populations. A: SEC separation of monomers, small oligomers and large oligomers. An expanded region of the oligomer populations is included. B: Pore-limit native gel-electrophoresis of fractionated small and large oligomers. C: SEC-MALLS analysis of the oligomer populations measured with 90° light scattering and 280 nm absorbance. The M_w of large oligomers, small oligomers and monomers estimated with MALLS is shown. D: Hydrodynamic radii estimated with SEC-DLS are shown together with refractive index and 90° light scattering.

accumulate under conditions where amyloid fibrils are formed and which can be isolated. We have analyzed the structure and size distribution of these oligomers using size-exclusion chromatography coupled with online multiangle laser light scattering (SEC-MALLS) and dynamic light scattering (SEC-DLS), native gel electrophoresis, transmission electron microscopy (TEM), atomic force microscopy (AFM), small-angle X-ray scattering (SAXS), Fourier transform infrared (FTIR), and circular dichroism (CD) spectroscopy. We identify two different oligomer populations which differ significantly in size but are structurally similar. Both oligomer populations are significantly more potent in membrane permeabilization than the monomers and fibrils. The small oligomers, which are most highly populated, on average consist of ∼30 monomers. These appear to form an ellipsoidal structure with a compact core and a less highly structured corona, each making up 50% of the total mass. Using an optimized thioflavin T (ThT) aggregation assay,[44,45] we show that the oligomers inhibit fibril formation in a concentration-dependent manner. The ThT time profiles can be fitted by a kinetic model in which the oligomers inhibit both the initial nucleation and the subsequent elongation steps. We also use a quartz crystal microbalance with dissipation monitoring (QCM-D), previously shown to be an excellent method to monitor fibril growth accurately,[46−48] and confirm that isolated oligomers, unlike αSN monomers, are not able to elongate preformed fibrils significantly.

MATERIALS AND METHODS

Protein Production and Handling. Freshly dissolved αSN was filtered (0.2 μm) prior to use, and the concentration determined by absorption measurements with a NanoDrop spectrophotometer (ND-1000, Thermo Scientific) using a theoretical extinction coefficient of 5960 M^{-1} cm^{-1}. All experiments were conducted in phosphate saline buffer (PBS) (20 mM phosphate, 150 mM NaCl, pH 7.4). Details of protein purification, oligomer purification, QCM-D, SEC-MALLS, SEC-DLS, and SAXS are provided in Supporting Information.

Plate Reader Fibril Formation Assays. ThT fluorescence was monitored using a 96-well plate reader setup as described previously.[44]

Pore Limit Gel Electrophoresis. The oligomers were analyzed by pore limit gel electrophoresis in the presence of Tris, boric acid, and EDTA system, as described previously.[49] In short, the samples were prepared under non-denaturing conditions (the addition of SDS and dithiothreitol was omitted) and separated by non-denaturing PAGE for 17 h at 100 V, using 4−20% gradient gels (10 × 10 × 0.15 cm^3). Oligomers were visualized by Coomassie Blue staining.

CD Spectroscopy. Far-UV wavelength spectra of αSN monomers, oligomers, and fibrils with protein concentrations of 0.2 mg/mL (14 μM) in a 1 mm cuvette were obtained at 25 °C with a Jasco J-810 spectrophotometer (Jasco Spectroscopic Co. Ltd., Japan). Prior to CD analysis, fibril solutions were sonicated 3 × 10 s on ice with an HD 2070 Bandelin Sonuplus Sonicator (Buch and Holm, Herlev, Denmark).

ATR-FTIR Spectroscopy. FTIR measurements were carried out with a Tensor 27 FTIR (Bruker Optics, Billerica, MA). Two μL samples were loaded onto the crystal and carefully dried with nitrogen gas. Spectra were accumulations of 68 scans, measured with a resolution of 2 cm^{-1} in the range from 1000 to 3998 cm^{-1}. Data processing, consisting of atmospheric compensation, baseline subtraction, deconvolution with Lorentzian curves, and second derivative analysis, was performed with the software OPUS version 5.5 (http://www.stsci.edu/software/OPUS/kona2.html). For comparison all absorbance spectra were normalized.

Transmission Electron Microscopy. Five μL aliquots of 0.2−0.4 mg/mL αSN in PBS buffer were transferred to 400-mesh carbon-coated, glow-discharged grids for 30 s. The grids were washed using

dx.doi.org/10.1021/ja411577t | J. Am. Chem. Soc. 2014, 136, 3859−3868

two drops of doubly distilled water, stained with 1% phosphotungstic acid (pH 6.8) and blotted dry on filter paper. The samples were viewed in a microscope (JEM-1010; JEOL, Tokyo, Japan) operating at 60 kV. Images were obtained using an Olympus KeenViewG2 camera.

Dye Leakage Measurements. Dioleoyl-phosphatidylglycerol (DOPG) vesicles with a diameter of 100 nm containing 70 mM calcein and in PBD buffer (pH 7.4) were prepared by extrusion as described previously.[50] αSN monomers, oligomers, and fibrils were each mixed in appropriate concentrations and loaded in a 96-well plate (Nunc, Thermo Fischer Scientific, Roskilde, Denmark) in triplicates. Calcein release was measured (excitation 485 nm; emission 520 nm) over 2 h in a Genios Pro fluorescence plate reader (Tecan, Männerdorf, Switzerland) at 37 °C with 2 s shaking every 2 min. Finally, Triton X-100 (0.1% (w/v)) was added to obtain 100% calcein release. The saturated calcein levels after 2 h were corrected for background fluorescence, and the % calcein release calculated.

Kinetic Model. We consider an aggregation mechanism which includes primary nucleation, and fibril elongation, and depolymerization events characterized by reaction rate constants k_n, k_+ and k_{off}, respectively. In addition, since aggregation is induced under shaking conditions we expect that secondary nucleation events related to fibril fragmentation will also be important and are characterized by a rate constant k_2. The kinetic equation governing the formation of fibril mass during time, $M(t)$, is given by:[51,52]

$$\frac{M(t)}{M(\infty)} = 1 - \exp(-C_+ e^{\kappa t} + C_- e^{-\kappa t} + D) \quad (1)$$

where $M(\infty)$ is the fibril mass in the long-time limit, and the constants are given as:

$$\kappa = \sqrt{2(m_0 k_+ - k_{off})k_2} \approx \sqrt{2m_0^{n_2+1}k_+k_2} \quad (2)$$

$$\lambda = \sqrt{2k_+k_n m_0^{n_c}} \quad (3)$$

$$C_\pm = \frac{\lambda^2}{2\kappa^2} \pm \frac{k_+P_0}{\kappa} \pm \frac{k_+M_0}{2(m_0k_+ - k_{off})} \approx \frac{\lambda^2}{2\kappa^2} \pm \frac{k_+M_0}{\kappa\bar{L}} \pm \frac{M_0}{2m_0} \quad (4)$$

$$D = \frac{\lambda^2}{\kappa^2} - \frac{M_0}{M(\infty)} + \frac{k_+M_0}{(m_0k_+ - k_{off})} \approx \frac{\lambda^2}{2\kappa^2} - \frac{M_0}{M(\infty)} + \frac{M_0}{m_0} \quad (5)$$

where m_0, M_0, and P_0 are, respectively, the monomer, the seed mass, and the seed number concentrations at time zero. The seed mass and number concentrations are connected via the average fibril length, $\bar{L} = M_0/P_0$.

Surface Tension Measurements. The effects of monomers and oligomers on the surface tension were analyzed with the pendant drop method using a KSV CAM 101 surface tension meter (KSV Instruments Ltd.). For every protein concentration, three different drops were measured, and 20 pictures were obtained from each drop. The surface tension was determined by fitting the drop shape with the CAM software (KSV Instruments Ltd.).

RESULTS

Both Types of αSN Oligomers Have a Distribution of Sizes. In accordance with our previous approach to optimize αSN oligomer formation,[1] oligomers were prepared by incubation of monomeric αSN at 12 mg/mL for 5 h. The Superose 6 matrix was able to separate monomers from two distinct oligomer populations eluting around ∼14.8 and ∼19.4 min (Figure 1A). In the following discussion, we refer to these two populations as the large and small oligomers, respectively. Typically, the small and large oligomers formed, respectively, 2−5% and <1% of the total αSN population. Based on the elution times of known globular proteins, we estimated the M_r to be 1812 ± 60 kDa for the small oligomers and 67 ± 11 kDa (n = 3) for the monomers (since monomeric αSN is natively unfolded, its size will be overestimated by all methods which rely on hydrodynamic volume). We were not able to estimate the M_r of the large oligomers, which elute at, or close to, the exclusion limit (∼4 × 10^4 kDa) of the SEC matrix (Figure 1A,C,D). Superdex 120 and 200 (exclusion limits at ∼100 and ∼1300 kDa, respectively) matrices were found to separate monomers from oligomers but were unable to separate the small and large oligomers which both eluted in the exclusion limits.[1,53]

The two oligomer populations also could not be separated by conventional gel electrophoresis techniques and pore limit gel-electrophoresis (PLGE), which are optimized for separation of large proteins. However, SEC followed by nondenaturing PLGE (Figure 1B) revealed a smear of sizes ≥ ∼670 kDa for the small oligomers. The large oligomers migrated as a much narrower band, an effect likely to be caused by the limited pore size of the gel.

To determine the sizes of the two types of oligomers independently of their hydrodynamic volume, we combined SEC with multiangle laser light scattering (MALLS) (Figure 1C). Consistent with the Superose 6 matrix exclusion limit of ∼4 × 10^4 kDa for globular proteins, size species exceeding 10^4 kDa occur in the void volume with a weight-averaged M_w of (5.8 ± 3.3) × 10^3 kDa (n = 6) and thus in the upper range of the optimal separation range of the separation medium (5−5 × 10^3 kDa). M_w estimates of the smaller oligomer population ranged from ∼310 ± 90 to 770 ± 210 kDa with a weight-averaged value (based on 7 individual runs) of 430 ± 88 kDa (n = 7) across the peak, corresponding to 30 ± 6 αSN monomers in each oligomer. The small oligomers' range of molecular weights reflects the inherent size separating properties of the column.

SEC-DLS was used to estimate the hydrodynamic radius (R_h) of eluting oligomer species (Figure 1D). Aggregate sizes >100 nm in hydrodynamic radius (well in excess of the Superose 6 pore size of ∼40 nm) were observed in the void volume, quickly declining to ∼30 nm. R_h values of ∼19 and ∼11 nm were obtained from the peak maxima for the large and small oligomers, respectively (Figure 1D).

TEM pictures of isolated small oligomers as well as large oligomers show that the small oligomers are generally spherical (Figure 2A), while the large oligomers are distinctly elongated and coexist with occasional short fibrils of length ∼150−300 nm (Figure 2B). AFM analysis of the small oligomers revealed a disc shape structure with an average height of 1−2 nm (Figure 2C). Protein aggregates with a loose structure are expected to collapse when they are dried on mica, so the apparent small height is probably caused by drying artifacts.

Small and Large Oligomers Have a Similar Secondary Structure Content That Differs from Those of Both Monomers and Fibrils. The secondary structures of the small and large oligomers are identical when analyzed by FTIR and CD (Figure S1). This similarity is remarkable, given their substantial size difference. The monomer has an absorption maximum in the amide I region of the FTIR spectrum at 1657 cm^{-1} (Figure 3A) as determined by second derivative analysis (data not shown); this wavelength corresponds to disordered structure.[54−56] Reference spectra of well-defined random coil proteins in H_2O have a band at 1660−1642 cm^{-1} with a maximum at 1654 cm^{-1}.[56] α-Helices also absorb within this region (1660−1648 cm^{-1}), but H/D exchange band shift analysis has previously shown that the band for αSN monomers

dx.doi.org/10.1021/ja411577t | J. Am. Chem. Soc. 2014, 136, 3859−3868

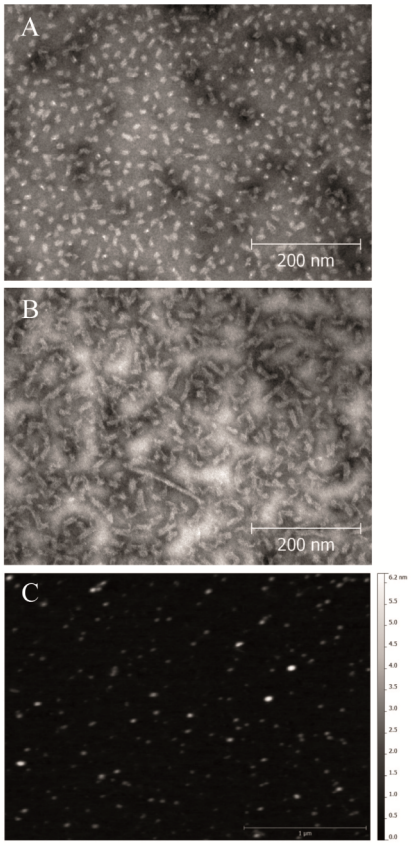

Figure 2. Structure analysis of the small oligomers. TEM images of (A) small and (B) large oligomers. (C) AFM images of the small oligomers with the height given as *Z*-scale.

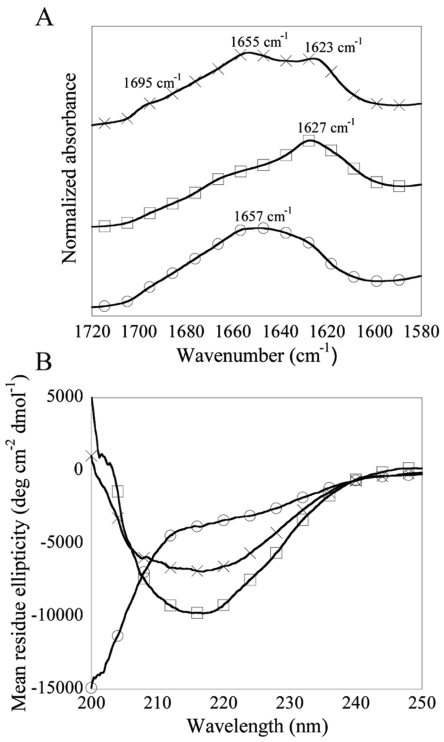

Figure 3. Analysis using (A) FTIR and (B) CD of monomers (○), fibrils (□), and small oligomers (×). In the FTIR spectra the peak maximum, determined with secondary derivative analysis, is indicated, and the spectra are displaced for better comparison.

in this region can be assigned to disordered structure.[56] Previous FTIR analysis demonstrates that the oligomers are likely to consist of antiparallel β-sheets and fibrils of parallel β-sheets.[55] Our oligomer and fibril FTIR spectra (Figures 3A and S1) are in good agreement with similar data reported by Raussens and co-workers, who use comparable methods to prepare oligomers.[12,55,57,58] The oligomer spectrum shows a maximum at 1655 cm^{-1}, indicative of a significant degree of disordered structure,[54,56] while the peak maximum at 1623 cm^{-1} and a weak but significant contribution at 1695 cm^{-1} (Figure 3A) both suggest antiparallel β-sheet structure.[55] Thus FTIR spectra support the combination of compact and extended structure predicted by our SAXS data, see later.

Far-UV CD analysis also reveals that the spectra of the two oligomers differ from those of both monomers and fibrils (Figure 3B). That of the monomers resembles the classical spectrum of an unstructured protein. The oligomer and fibril spectra differ clearly in the intensity of different wavelengths, although both have a minimum at 217 nm, which, in conjunction with the absence of minima at 208 and 222 nm, indicates the presence of β-sheet rather than α-helical structure. The secondary structure composition of the oligomers could not be estimated using conventional fitting programs due to the poor quality of data below 200 nm. Nor could the oligomer spectra be reconstructed by linear combinations of the monomer and fibril spectra (deviations were particularly pronounced around 200−210 nm), indicating that the oligomers exist as distinct species.

Both Oligomers Bind ANS. The fluorophore 1-anilinonaphthalene-8-sulfonate (ANS) has been found to show binding specificity toward a variety of amyloid oligomers.[59] In the present study, both fibrils and oligomers were found to increase ANS fluorescence emission intensity and to generate a blueshift significantly larger than that of monomer (although the shift in λ_{max} of fibrils and oligomers is less pronounced than previously observed).[59] Fibrils lead to higher ANS intensity but to a smaller ANS blueshift (Figure S4), indicating that the nature of the ANS binding sites is different in the oligomers and the fibrils. As with the FTIR and CD data, ANS fluorescence intensity and λ_{max} in the presence of the small and large oligomers are identical (Figure S4).

Both Oligomers Permeabilize Vesicles. Both small and large oligomers are significantly more potent in inducing the loss of calcein from inside vesicles than the monomers (Figure 4). We estimate that the stoichiometric potency of the small oligomers to disrupt vesicles is ∼500, i.e., one oligomer is as potent in inducing calcein release as ∼500 monomers (Table 1). The fibrils are significantly less potent than the oligomers, see Figure S5 and Table 1. The high reproducibilities of both the dye leakage experiments and the oligomer preparations are revealed by the small standard deviation of the potency values, based on two separate experimental series (Table 1).

SAXS Data of the Small Oligomers Indicate an Ellipsoid with a Rim of Flexible Protein Molecules. More detailed data on oligomer structure and size estimates were obtained from SAXS. Our analysis has been limited to the small oligomers, since it is not possible to purify the large oligomers to sufficiently high concentrations for these experiments. SAXS data for αSN monomers and the small oligomers are presented in Figure 5A together with the best fits of the

dx.doi.org/10.1021/ja411577t | J. Am. Chem. Soc. 2014, 136, 3859−3868

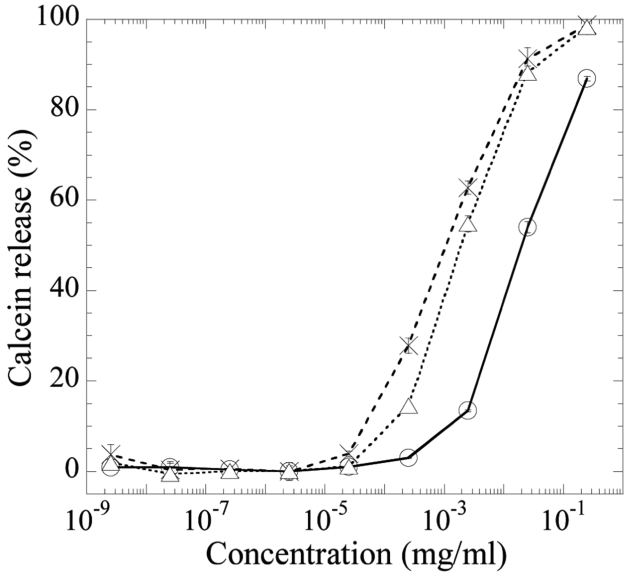

Figure 4. Calcein release of DOPG vesicles (100 nm diameter) by small oligomers (×), large oligomers (△), and monomers (○). 100% represents complete permeabilization of vesicles which is reached by addition of the detergent Triton X-100. Data points are averaged triplicates, and standard deviation is given.

Table 1. Ability of Different αSN Species to Release Calcein from Vesicles[a]

species	$C_{50\%}$ (mg/mL)[b]	$C_{50\%}$ (μM, monomer)	relative potency (concentration)[c]	relative potency (stoichiometric)[d]
monomer	0.019	1.31	1	1
small oligomers	0.001	0.08	17	~500
large oligomers	0.002	0.14	9	N/A
fibrils	N/A	N/A	3	N/A

[a]We estimate ~10% deviation on the relative potency when comparing distinct experimental series. [b]Concentration needed for 50% calcein release. Estimated by fitting data in Figure 4 to a sigmoidal function. [c]Defined as $C_{50\%}$(species)/$C_{50\%}$(monomer) (columns 2 and 3). [d]As footnote b but based on the molar concentration of oligomer.

models described as a function of the modulus of the scattering vector, given by $q = 4\sin(\theta)/\lambda$, where 2θ is the scattering angle and $\lambda = 1.54$ Å is the wavelength of the X-ray radiation. A first indication of the shape is provided by the model-independent $p(r)$ functions of the two data sets (Figure 5B), which reflect the distribution of internal distances in the particles.[60]

The monomer data are those expected for a random coil with a maximum around R_g and a tail at larger distances. The R_g value of 4.23 ± 0.11 nm is in good agreement with previously published values.[61,62] Independent fitting of the monomer data to a random coil model[63] gives an R_G of 4.20 ± 0.05 nm. The correspondence of R_G values between these two approaches emphasizes that αSN is an intrinsically disordered protein, consistent with the literature.[64]

While the symmetric bell shape of the $p(r)$ function for the oligomers suggests some nonrandom structure, it also shows a rather long tail, indicative of a random coil. Indeed, the linear appearance of the spectrum at high q values in a double logarithmic plot (seen for the oligomer at $q > 0.08$ Å^{-1}, Figure 5A) typically originates from the scattering from disordered structure (q^{-2}). Combining these two types of structures, we

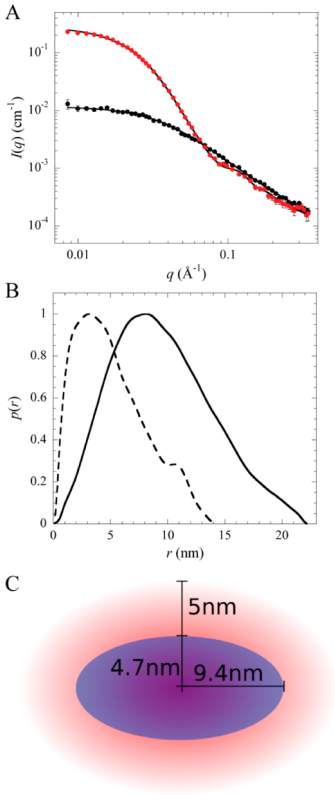

Figure 5. SAXS analysis of the small oligomers. (A) SAXS data of monomers (■) and oligomers (●) with the best fit to data of the models described in the text. The data are normalized to a concentration of 1 mg/mL. (B) $p(r)$ functions of the monomer (dashed line) and oligomer (continuous line) data, normalized so the maximum value is equal to unity. (C) Schematic representation of the oligomer model predicted from SAXS data.

find that the best model to fit the oligomer data consists of a core in the shape of a prolate ellipsoid (ellipse rotated around its major axis, dimensions R, R, εR, where ε is the width:height aspect ratio) with a rim of flexible protein molecules,[65] as presented schematically in Figure 5C. Note that despite a mass polydispersity in the range of 50% measured by MALLS, we obtain a good fit to our SAXS data using a monodisperse model. Size polydispersity will be significantly lower than mass polydispersity.

We expect the number of polypeptide chains in the model of the SAXS data (q dependence) to correspond to the experimentally determined number of molecules in the oligomer. This number has been determined from the forward scattering intensity, which provides the M_w of the complexes if the concentration is known. From the forward scattering, we estimate the M_w of the oligomers to be ~420 kDa, which corresponds to ~29 monomers per oligomer, in excellent agreement with the SEC-MALLS estimation of 30 ± 6 monomers. The results of the fit of the prolate ellipsoidal model fit to the oligomer data give $R = 4.72 \pm 0.17$ nm and $\varepsilon = 1.99 \pm 0.19$, while the radius of gyration of the attached coils is $R_g = 2.48 \pm 0.19$ nm. From the fit, the number of chains in the model is 21.1 ± 3.3 nm, which is broadly similar to the number expected from the forward scattering (30 ± 6). The fraction of scattering length in the chains (which in this model corresponds to the volume or mass fraction of protein) is 0.46 ± 0.02, indicating that around half of the protein is present in the flexible regions of the shell.

dx.doi.org/10.1021/ja411577t | J. Am. Chem. Soc. 2014, 136, 3859−3868

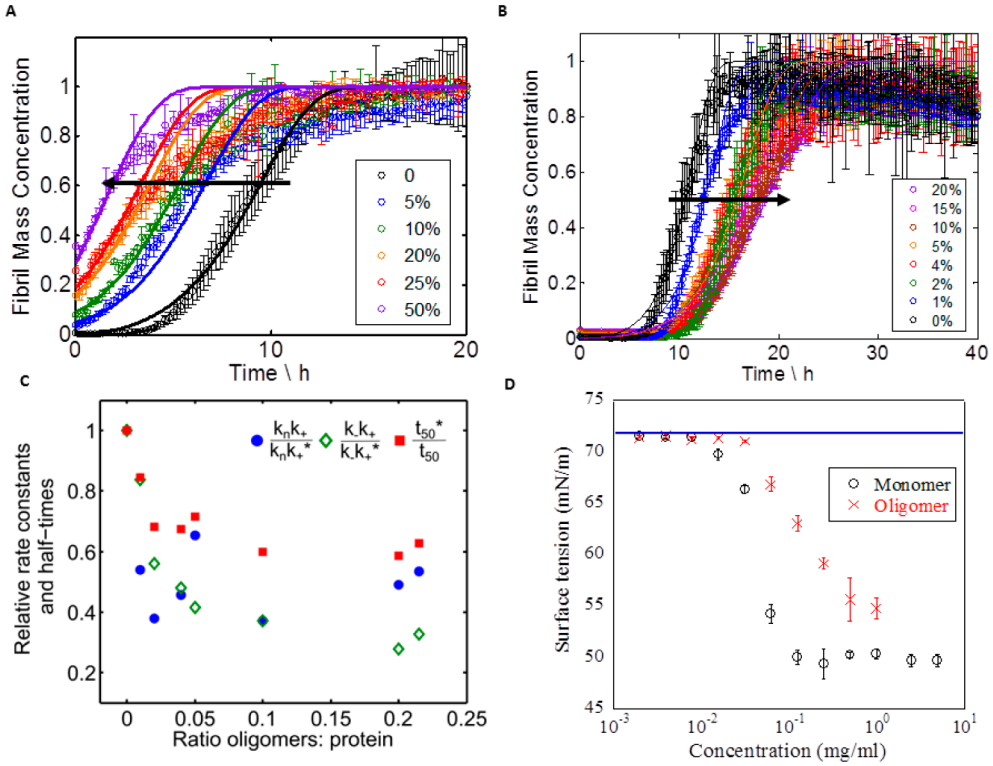

Figure 6. Kinetic analysis of the ability of the oligomers to inhibit fibril formation. (A) Seeding experiments with 1 mg/mL monomer and increasing amount of seeds (5; 10; 20; 25; 50% of monomer concentration) as indicated by the arrow. The continuous lines represent a global fit. (B) Kinetic traces of 1 mg/mL monomer with increasing oligomer concentrations. The arrow indicates the increasing concentration of oligomers: (1; 2; 4; 5; 10; 15; 20% of monomer concentration). The continuous lines represent model calculations. (C) The microscopic rate constants (primary nucleation, k_n, elongation, k_+, and secondary nucleation, k_2, rate constants) corresponding to the model calculations in (B) as well as the half times (t_{50}) relative to the values in the absence of oligomers (indicated by the symbol *) are plotted as a function of the oligomer concentration. The concentration of monomer is 1 mg/mL, thus the ratios also indicate the oligomer concentration in mg/mL. The inhibitory effect of the oligomers reaches saturation at a critical oligomer concentration of about 0.05 mg/mL. (D) Surface tension values as a function of monomer and oligomer concentrations. The blue line indicate the surface tension of buffer with no protein.

The Presence of the Oligomers Alters the Aggregation Kinetics. To explore the role of the oligomers studied here in the process of amyloid fibril formation, we have analyzed their effects on the kinetics of fibril formation and of fibril elongation. To obtain as high a concentration of oligomers as possible, we purified the oligomers after incubating them under fibril forming conditions (12 mg/mL αSN for 5 h) and analyzed their effects in aggregation assays at 1 mg/mL. We obtained a similar fraction of oligomers at 1, 5, and 12 mg/mL (Figure S5A). Moreover, fibrils formed at 1 and 12 mg/mL have the same FTIR and CD spectra (Figure S2) and the same vesicle permeabilization potency (Figure S5). To elucidate the roles of the oligomers in the aggregation pathway of αSN, we investigated the influence of the oligomers on the aggregation kinetics. We were unable to purify sufficient quantities of the large oligomer for these experiments and confine ourselves to using a mixture of small and large oligomers (similar effects are seen for the small oligomers alone, implying that the two oligomers have essentially the same effect).

Seeding has been widely used to bypass the primary nucleation step of amyloid fibril formation.[16] When adding sonicated preformed αSN fibrils (seeds) to monomers, aggregation is rapid (Figure 6A). We can describe quantitatively the effects of the variation in seed concentration on the aggregation kinetics by applying theoretical analysis.[51,52,66,67] Since aggregation occurs under conditions of strong shaking, we included secondary nucleation induced by breakage together with primary nucleation and elongation as microscopic processes. The global fit of the data to such a model shows that it is able to explain the data quantitatively (Figure 6A).[16]

To test whether the oligomers are able to accelerate the aggregation process in a fashion similar to the seed fibrils, we added different concentrations of oligomers to solutions of the monomeric protein. Remarkably, the oligomers do not shorten or eliminate the lag phase, as is the case for seed fibrils; rather, the oligomers lead to longer lag phases in a concentration-dependent manner (Figure 6B). To rationalize this finding, we have fitted this data set to a model that allows for inhibition of the individual molecular steps, through semiempirical rate constants which do not specifically include the oligomer but provide values for the rate constants associated with the individual molecular steps at different oligomer concentrations. The global fit together with the experimental data are shown in Figure 6B, and the corresponding microscopic kinetic rate constants are reported in Figure 6C together with the experimental half-times. This analysis suggests that the oligomers may reduce both the primary nucleation and the elongation rate to an extent which reaches saturation at a critical oligomer concentration of about 0.1 mg/mL. The oligomer surface tension levels off at slightly higher concentrations (Figure 6D). Increasing the oligomer concentration above the critical value does not further affect the aggregation kinetics.

dx.doi.org/10.1021/ja411577t | J. Am. Chem. Soc. 2014, 136, 3859−3868

To ensure that the inhibitory effect of the oligomers is not simply the effect of a decrease in the monomer concentration due to its sequestration by oligomers, we performed a simple binding assay (Figure S6). We incubated monomers and oligomers for 1 h under fibril forming conditions and compared the levels of the monomers and the oligomers before and after this procedure. Incubation with oligomers did not lead to any significant change in the monomer or oligomer concentrations nor to any differences in the area of the oligomer peak (Table S1; Figure S6), indicating that any sequestration was insignificant.

αSN Oligomers Do Not Elongate Fibrils. We used the ThT fluorescence assay to determine whether or not the oligomers are able to elongate fibril seeds. When preformed seed fibrils were incubated with oligomers, hardly any increase in fluorescence was observed, whereas monomers at the same mass/volume concentration yielded the expected increase in fluorescence (Figure 7A). This result suggests that the oligomers do not incorporate into fibrils to a significant extent.

To rule out that ThT-negative aggregates were formed upon interaction between oligomers and seed fibrils, we attached αSN fibril seeds on a sensor surface[68] and used QCM-D to monitor fibril growth directly, based on changes in the resonant frequency (Δf) of the sensor crystal.[46,48,69] To a first approximation, Δf is proportional to the change in the mass deposited on the crystal. First, all four channels were subjected to two injections of 20 μM freshly prepared monomer solution separated by a washing step. This procedure consistently led to essentially linear decreases in the resonant frequency (Figure 7B), suggesting addition of monomers to the growing end(s) of fibrils attached to the sensor surface. The same fibril-loaded sensors were then either incubated again with a solution of 20 μM (0.28 mg/mL) monomer or with one containing the same mass concentration (0.28 mg/mL) of oligomers to examine the possible interaction of oligomers with attached fibrils.

While monomers efficiently elongated the attached fibrils, we consistently observed at most very small changes in resonant frequency when the sensors were incubated with oligomers; indeed the small Δf (as well as the small rise in ThT fluorescence in Figure 7A) may be attributed to a small quantity of monomer in equilibrium with the oligomer preparation, as identified by analytical SEC of prepurified oligomers (Figure S6). QCM dissipation data, which can be found in Figures S8 and S9 confirm the frequency data. There is essentially a linear relationship between Δf and dissipation (Figure S10), supporting the interpretation that Δf is directly associated with seed fibril elongation and not with differences in viscoelastic properties of the fibril layer.

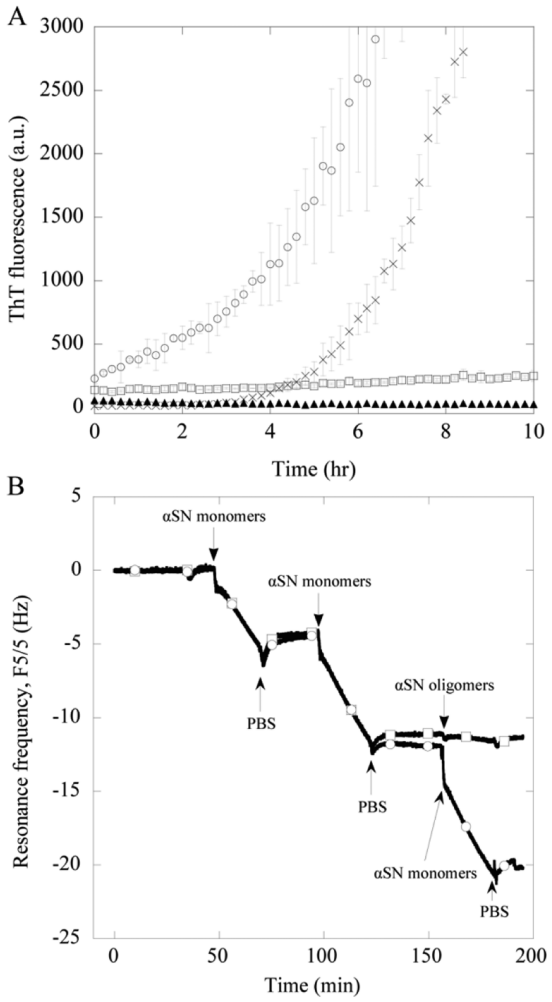

Figure 7. Kinetic analysis of the ability of oligomers to elongate seeds. (A) Kinetic traces of fibril formation followed by observing ThT fluorescence of the following: 0.7 μM seeds (▲); 0.7 μM seeds and 35 μM oligomers (□), 0.7 μM seeds and 35 μM monomers (○), and 35 μM monomers (×). All data points are averaged triplicates and the standard deviations are shown. (B) Direct monitoring of fibril growth by QCM-D with dissipation upon injection of 2 × 20 μM αSN monomers and either 20 μM AS monomers (□) or 20 μM αSN oligomers (○) separated by PBS washes. The experiment was repeated three times with qualitatively similar results.

DISCUSSION

The Small αSN Oligomers Consist of ∼30 Molecules and Contain Significant Amounts of Unstructured Regions. SEC, gel electrophoresis, and TEM show that αSN forms two distinct oligomer populations, and AFM confirms the spherical shape of the small oligomers observed with TEM. FTIR and CD measurements reveal that the small and large oligomers have similar secondary structure, distinct from both monomers and fibrils. Furthermore, both oligomer populations induce more vesicle permeabilization than monomers and fibrils (Table 1) and give a similar response to the fluorophore ANS (Figure S3).

M_w values of unstructured proteins are overestimated by methods relying on hydrodynamic volume, such as SEC. In the case of the 14.5 kDa αSN this effect leads to a 4-fold overestimate (67 ± 11 kDa). However, when SEC is combined with MALLS, a reliable estimate (15 ± 3 kDa) can be obtained which also agrees well with SAXS data (17.9 kDa). In the case of the small oligomers, the high quality of the SAXS fit (based on the assumption of a single species) indicates that there is limited polydispersity in our samples, consistent with the relatively narrow SEC peak for the small oligomer. SEC-MALLS and SAXS give estimates of the size of the small oligomers as 430 ± 88 and 420 kDa, respectively, corresponding to ∼30 monomers per oligomer. This result is in good agreement with a single-molecule photobleaching study by Subramaniam and co-workers in which the number of monomers in stable and well-defined αSN oligomers was determined to be 31.[70] The higher estimates of the M_w of the small oligomers from SEC and gel electrophoresis (1812 ± 60 and 670 kDa, respectively) suggest the presence of a degree of extended structure; this conclusion is consistent with our SAXS

dx.doi.org/10.1021/ja411577t | J. Am. Chem. Soc. 2014, 136, 3859−3868

based model, where a compact ellipsoidal core (50% of the mass) is surrounded by an outer rim of flexible regions of polypeptide chains (also 50% of the mass). The dimensions of the SAXS-based model, a width of 15 nm and a height of 10 nm (Figure 5C), are in good agreement with SEC-DLS data where the average R_h is determined to be 11 nm. Both CD and FTIR show a strong β-sheet signal, which FTIR suggests is organized in antiparallel β-sheets. The FTIR data also suggest a significant contribution from disordered polypeptide structure, consistent with the flexible outer rim discussed above.

Comparisons with Previous Investigations of Oligomer Structure. We have previously followed the process of fibril formation of αSN by SAXS, in which we obtained spectra of the complete mixture of species present during aggregation.[1] We were able to decompose these spectra to obtain contributions from monomers/dimers, oligomers, and fibrils and to propose an ellipsoidal model for the oligomeric species. That model lacked a flexible outer layer, but its width:height dimensions (4.5:9.0 nm) are similar to the dimensions of the core of the oligomer structure determined in the present study (4.7:9.4 nm). The absence of an outer layer in the previous model most likely reflects the challenges of extracting data for individual species from mixtures; in contrast, the present study is based on purified species. We consider it unlikely that the process of purifying the oligomers should lead to structural changes such as the formation of an unstructured outer layer. Consistent with this conclusion, we do not observe from CD spectra any structural rearrangements in the oligomers during concentration of the sample (data not shown), and both concentrated and nonconcentrated oligomers have a similar inhibitory effect on amyloid formation. In addition, concentrated small oligomers have the same M_w, as determined by SAXS as nonconcentrated small oligomers analyzed by SEC-MALLS.

Oligomers Induce Greater Perturbation in Membranes than Monomer. The ability of the N-terminus of the αSN monomer to fold into a helical conformation upon interaction with anionic vesicles is well described in the literature.[71−73] The N-terminal part of αSN (residues 1−60) is highly basic with a pI of 9.5, and electrostatic interactions with this part of the protein are believed to drive interaction with anionic vesicles. In the dye leakage experiment (Figures 4 and S4) we found that ∼500 monomers are needed to cause the same degree of calcein release as a single small oligomer (consisting of ∼30 monomers). We suggest two possible mutually reinforcing reasons for oligomer potency. First, the initial 10−20 residues in the N-terminus could be disordered in the oligomers and located primarily in the outer rim. The N-terminus has previously been shown to be important for the interactions of oligomers with membranes,[74] and we have demonstrated the importance of the initial 11 residues on the oligomers ability to interact with and permeabilize membranes.[53] The simultaneous binding of several proximal N-termini to a vesicle would be expected to induce a high degree of disruption. In contrast, the monomers will be widely distributed in the membrane due to diffusion and electrostatic repulsion and are likely to bind more weakly, requiring higher concentrations to cause the same extent of release as oligomers. Second, the hydrophobic core of the oligomers which binds ANS (Figure S3) might be included in the vesicle interactions and could lead to a stronger interaction and increased permeability. The lowered potency of fibrils may reflect that it is mainly the ends of the fibrils that interact with membranes[75,76] and in addition that much of the polypeptide chain is buried in the highly ordered structure. Nevertheless, fibrils are not completely inert, and at the stoichiometric level (but not in terms of mass units), one fibril might be more toxic than one oligomer, as proposed recently.[77,78]

Oligomers Are Not Able to Elongate Seed Fibrils and They Do Not Act As Seeds. Our data analysis demonstrates that, whereas sonicated fibrils (seeds) initiate the aggregation process efficiently through recruitment of monomers to the growth-competent ends, oligomers have an inhibitory effect, prolonging the lag time in a concentration dependent manner. There is no significant sequestration of monomers by oligomers, i.e., the oligomers do not prolong lag times by decreasing (or increasing) the effective monomer concentration, and QCM-D fails to detect direct interactions between oligomers and fibrils. The inhibitory effect on fibril formation reaches saturation at a critical oligomer concentration of ∼0.1 mg/mL, which is only slightly below the onset of the saturation in the decrease of surface tension with increasing oligomer concentration. This observation, together with evidence in the literature on the effect of air−water interfaces on αSN aggregation,[79−81] suggests that the critical oligomer concentration represents the point at which the interface is saturated with oligomers. The monomers and the oligomers therefore compete for the air−water interface, where primary nucleation of the aggregation process is likely to occur. Furthermore, we find that the oligomers are not able to elongate seed fibrils detectably.

We can refine our modeling even further: In a recent single molecule study, the characteristic time scale of rearrangement of one type of αSN oligomer into another type was determined to be of the order of 5×10^{-5} s^{-1}.[82] If we assume that the oligomers in the present study have to rearrange with a rate constant of this order of magnitude after attachment to a fibril end in order to create a template for further attachment, we find that fibril growth by oligomer addition is 2−3 orders of magnitude less efficient than growth by monomer addition (Buell et al. in revision; see Figure S7 for details on the calculation).

Our previous SAXS study showed that oligomers of the type investigated here are mainly observed during the growth phase of fibril formation at a protein concentration of 12 mg/mL and disappear at the completion of the aggregation process,[1] leading to our earlier suggestion that oligomers are the elongating species in the aggregation process. The present data, however, suggests instead that the disappearance of the small oligomers at the end of an aggregation reaction is due to their self-aggregation into much larger aggregates, as seen upon prolonged incubation (data not shown), or by dissociation into monomers as the concentration of the latter becomes depleted. The fact that we do not observe any other well-defined species between the monomers and the oligomers containing ∼30 αSN molecules by means of SEC, SEC-MALLS, or gel electrophoresis (data not shown) is consistent with monomers being the species which elongate αSN fibrils, as shown previously by analysis of the kinetics of aggregation (Buell et al. in revision).

In summary, we have characterized the form of the αSN oligomer that is most prevalent under conditions where amyloid fibril formation is observed. The oligomers consist of an average of ∼30 monomers and have an ellipsoidal structure, consistent with our previous SAXS study.[1] We find that the compact core is organized in β-sheet structure and that ∼50%

of the polypeptide chains are unstructured and located in an outer rim. These oligomers are unable to elongate fibrils to a significant extent and also do not act as seeds for fibril growth.

■ ASSOCIATED CONTENT

Supporting Information

Additional materials and methods as well as information about oligomer and fibril structure, ANS binding, membrane permeabilization, monomer sequestration, lack of oligomer self-association, and fibril elongation capacity. This material is available free of charge via the Internet at http://pubs.acs.org.

■ AUTHOR INFORMATION

Corresponding Author

dao@inano.au.dk

Present Addresses

[⊥]Department of Protein biophysics and formulation, Novo Nordisk A/S, 2760 Måløv, Denmark.

[#]Arla Foods Ingredients, R&D Nr. Vium, Sønderupvej 26, DK - 6920 Videbæk.

Notes

The authors declare no competing financial interest.

■ ACKNOWLEDGMENTS

N.L., S.B.N., B.S.V., M.A. and D.E.O are supported by the Michael J. Fox Foundation, the Danish Research Council (Industrial Postdoc and The Danish Council for Independent Research | Natural Sciences), and the Danish Research Foundation (inSPIN). J.D.K. acknowledges LUNDBECKFONDEN for financial support. A.K.B. thanks EMBO, Magdalene College, Cambridge, and the Leverhulme trust for support. C.M.D and T.P.J.K. thank the Wellcome trust and the BBSRC for funding. We thank Nunilo Cremades for helpful discussions.

■ REFERENCES

(1) Giehm L, S. D.; Otzen, D. E.; Vestergaard, B. *Proc. Natl. Acad. Sci. U.S.A.* **2011**, *108* (8), 3246.

(2) Lashuel, H. A.; Hartley, D.; Petre, B. M.; Walz, T.; Lansbury, P. T., Jr. *Nature* **2002**, *418*, 291.

(3) Conway, K. A.; Lee, S. J.; Rochet, J. C.; Ding, T. T.; Williamson, R. E.; Lansbury, P. T., Jr. *Proc. Natl. Acad. Sci. U.S.A.* **2000**, *97*, 571.

(4) Winner, B.; Jappelli, R.; Maji, S. K.; Desplats, P. A.; Boyer, L.; Aigner, S.; Hetzer, C.; Loher, T.; Vilar, M.; Campioni, S.; Tzitzilonis, C.; Soragni, A.; Jessberger, S.; Mira, H.; Consiglio, A.; Pham, E.; Masliah, E.; Gage, F. H.; Riek, R. *Proc. Natl. Acad. Sci. U.S.A.* **2011**, *108*, 4194.

(5) Walsh, D. M.; Selkoe, D. J. *J. Neurochem.* **2007**, *101*, 1172.

(6) Luheshi, L. M.; Tartaglia, G. G.; Brorsson, A. C.; Pawar, A. P.; Watson, I. E.; Chiti, F.; Vendruscolo, M.; Lomas, D. A.; Dobson, C. M.; Crowther, D. C. *PLoS Biol.* **2007**, *5*, e290.

(7) Dobson, C. M. *Nature* **2003**, *426*, 884.

(8) Lesne, S.; Koh, M. T.; Kotilinek, L.; Kayed, R.; Glabe, C. G.; Yang, A.; Gallagher, M.; Ashe, K. H. *Nature* **2006**, *440*, 352.

(9) Nilsberth, C.; Westlind-Danielsson, A.; Eckman, C. B.; Condron, M. M.; Axelman, K.; Forsell, C.; Stenh, C.; Luthman, J.; Teplow, D. B.; Younkin, S. G.; Naslund, J.; Lannfelt, L. *Nat. Neurosci.* **2001**, *4*, 887.

(10) Bernstein, S. L.; Dupuis, N. F.; Lazo, N. D.; Wyttenbach, T.; Condron, M. M.; Bitan, G.; Teplow, D. B.; Shea, J. E.; Ruotolo, B. T.; Robinson, C. V.; Bowers, M. T. *Nat. Chem.* **2009**, *1*, 326.

(11) Bucciantini, M.; Giannoni, E.; Chiti, F.; Baroni, F.; Formigli, L.; Zurdo, J.; Taddei, N.; Ramponi, G.; Dobson, C. M.; Stefani, M. *Nature* **2002**, *416*, 507.

(12) Volles, M. J.; Lee, S. J.; Rochet, J. C.; Shtilerman, M. D.; Ding, T. T.; Kessler, J. C.; Lansbury, P. T., Jr. *Biochemistry* **2001**, *40*, 7812.

(13) Chiti, F.; Dobson, C. M. *Annu. Rev. Biochem.* **2006**, *75*, 333.

(14) Hill, S. E.; Robinson, J.; Matthews, G.; Muschol, M. *Biophys. J.* **2009**, *96*, 3781.

(15) Vestergaard, B.; Groenning, M.; Roessle, M.; Kastrup, J. S.; van de Weert, M.; Flink, J. M.; Frokjaer, S.; Gajhede, M.; Svergun, D. I. *PLoS Biol.* **2007**, *5*, e134.

(16) Lorenzen, N.; Cohen, S. I. A.; Nielsen, S. B.; Herling, T. W.; Christiansen, G.; Dobson, C. M.; Knowles, T. P. J.; Otzen, D. *Biophys. J.* **2012**, *102*, 2167.

(17) Kardos, J.; Yamamoto, K.; Hasegawa, K.; Naiki, H.; Goto, Y. *J. Biol. Chem.* **2004**, *279*, 55308.

(18) Kim, H. J.; Chatani, E.; Goto, Y.; Paik, S. R. *J. Microbiol. Biotechnol.* **2007**, *17*, 2027.

(19) Knowles, T. P.; Fitzpatrick, A. W.; Meehan, S.; Mott, H. R.; Vendruscolo, M.; Dobson, C. M.; Welland, M. E. *Science* **2007**, *318*, 1900.

(20) Collins, S. R.; Douglass, A.; Vale, R. D.; Weissman, J. S. *PLoS Biol.* **2004**, *2*, 1582.

(21) Morris, A. M.; Watzky, M. A.; Finke, R. G. *Biochim. Biophys. Acta* **2009**, *1794*, 375.

(22) Jain, S.; Udgaonkar, J. B. *Biochemistry* **2011**, *50*, 1153.

(23) Necula, M.; Kayed, R.; Milton, S.; Glabe, C. G. *J. Biol. Chem.* **2007**, *282*, 10311.

(24) Souillac, P. O.; Uversky, V. N.; Millett, I. S.; Khurana, R.; Doniach, S.; Fink, A. L. *J. Biol. Chem.* **2002**, *277*, 12666.

(25) Gellermann, G. P.; Byrnes, H.; Striebinger, A.; Ullrich, K.; Mueller, R.; Hillen, H.; Barghorn, S. *Neurobiol. Dis.* **2008**, *30*, 212.

(26) Hong, D. P.; Han, S.; Fink, A. L.; Uversky, V. N. *Protein Pept. Lett.* **2011**, *18*, 230.

(27) Pedersen, J. S.; Dickov, D.; Flink, J. L.; Hjuler, H. A.; Christensen, G.; Otzen, D. E. *J. Mol. Biol.* **2006**, *355*, 501.

(28) Andersen, C. B.; Hicks, M. R.; Vetri, V.; Vandahl, B.; Rahbek-Nielsen, H.; Thogersen, H.; Thogersen, I. B.; Enghild, J. J.; Serpell, L. C.; Rischel, C.; Otzen, D. E. *J. Mol. Biol.* **2010**, *397*, 932.

(29) Ghodke, S.; Nielsen, S. B.; Christiansen, G.; Hjuler, H. A.; Flink, J.; Otzen, D. E. *FEBS J.* **2011**, *279*, 752.

(30) Sawaya, M. R.; Sambashivan, S.; Nelson, R.; Ivanova, M. I.; Sievers, S. A.; Apostol, M. I.; Thompson, M. J.; Balbirnie, M.; Wiltzius, J. J.; McFarlane, H. T.; Madsen, A. O.; Riekel, C.; Eisenberg, D. *Nature* **2007**, *447*, 453.

(31) Tycko, R. *Curr. Opin. Struct. Biol.* **2004**, *14*, 96.

(32) Nielsen, J. T.; Bjerring, M.; Jeppesen, M. D.; Pedersen, R. O.; Pedersen, J. M.; Hein, K. L.; Vosegaard, T.; Skrydstrup, T.; Otzen, D. E.; Nielsen, N. C. *Angew. Chem., Int. Ed. Engl.* **2009**, *48*, 2118.

(33) Jaroniec, C. P.; MacPhee, C. E.; Bajaj, V. S.; McMahon, M. T.; Dobson, C. M.; Griffin, R. G. *Proc. Natl. Acad. Sci. U.S.A.* **2004**, *101*, 711.

(34) Vilar, M.; Chou, H. T.; Luhrs, T.; Maji, S. K.; Riek-Loher, D.; Verel, R.; Manning, G.; Stahlberg, H.; Riek, R. *Proc. Natl. Acad. Sci. U.S.A.* **2008**, *105*, 8637.

(35) Fitzpatrick, A. W.; Debelouchina, G. T.; Bayro, M. J.; Clare, D. K.; Caporini, M. A.; Bajaj, V. S.; Jaroniec, C. P.; Wang, L.; Ladizhansky, V.; Muller, S. A.; Macphee, C. E.; Waudby, C. A.; Mott, H. R.; De Simone, A.; Knowles, T. P.; Saibil, H. R.; Vendruscolo, M.; Orlova, E. V.; Griffin, R. G.; Dobson, C. M. *Proc. Natl. Acad. Sci. U.S.A.* **2013**, *110*, 5468.

(36) Uversky, V. N. *FEBS J.* **2010**, *277*, 2940.

(37) Fandrich, M. *J. Mol. Biol.* **2012**, *421*, 427.

(38) Rosensweig, C.; Ono, K.; Murakami, K.; Lowenstein, D. K.; Bitan, G.; Teplow, D. B. *Methods Mol. Biol.* **2012**, *849*, 23.

(39) Sandberg, A.; Luheshi, L. M.; Sollvander, S.; Pereira de Barros, T.; Macao, B.; Knowles, T. P.; Biverstal, H.; Lendel, C.; Ekholm-Petterson, F.; Dubnovitsky, A.; Lannfelt, L.; Dobson, C. M.; Hard, T. *Proc. Natl. Acad. Sci. U.S.A.* **2010**, *107*, 15595.

(40) Polymeropoulos, M. H.; Higgins, J. J.; Golbe, L. I.; Johnson, W. G.; Ide, S. E.; Di Iorio, G.; Sanges, G.; Stenroos, E. S.; Pho, L. T.; Schaffer, A. A.; Lazzarini, A. M.; Nussbaum, R. L.; Duvoisin, R. C. *Science* **1996**, *274*, 1197.

(41) Spillantini, M. G.; Schmidt, M. L.; Lee, V. M.; Trojanowski, J. Q.; Jakes, R.; Goedert, M. *Nature* **1997**, *388*, 839.

(42) Spillantini, M. G.; Crowther, R. A.; Jakes, R.; Hasegawa, M.; Goedert, M. *Proc. Natl. Acad. Sci. U.S.A.* **1998**, *95*, 6469.
(43) Polymeropoulos, M. H.; Lavedan, C.; Leroy, E.; Ide, S. E.; Dehejia, A.; Dutra, A.; Pike, B.; Root, H.; Rubenstein, J.; Boyer, R.; Stenroos, E. S.; Chandrasekharappa, S.; Athanassiadou, A.; Papapetropoulos, T.; Johnson, W. G.; Lazzarini, A. M.; Duvoisin, R. C.; Di Iorio, G.; Golbe, L. I.; Nussbaum, R. L. *Science* **1997**, *276*, 2045.
(44) Giehm, L.; Otzen, D. E. *Anal. Biochem.* **2010**, *400*, 270.
(45) Levine, H. I. *Protein Sci.* **1993**, *2*, 404.
(46) Buell, A. K.; Dobson, C. M.; Welland, M. E. *Methods Mol. Biol.* **2012**, *849*, 101.
(47) Hovgaard, M. B.; Dong, M.; Otzen, D. E.; Besenbacher, F. *Biophys. J.* **2007**, *93*, 2162.
(48) Buell, A. K.; Dhulesia, A.; White, D. A.; Knowles, T. P.; Dobson, C. M.; Welland, M. E. *Angew. Chem., Int. Ed. Engl.* **2012**, *51*, 5247.
(49) Manwell, C. *Biochem. J.* **1977**, *165*, 487.
(50) Nesgaard, L.; Vad, B.; Christiansen, G.; Otzen, D. *Biochim. Biophys. Acta* **2009**, *1794*, 84.
(51) Cohen, S. I. A.; Vendruscolo, M.; Welland, M. E.; Dobson, C. M.; Terentjev, E. M.; Knowles, T. P. J. *J. Chem. Phys.* **2011**, *135*, 065105.
(52) Cohen, S. I. A.; Vendruscolo, M.; Dobson, C. M.; Knowles, T. P. J. *J. Chem. Phys.* **2011**, *135*, 065107.
(53) Lorenzen, N.; Lemminger, L.; Pedersen, J. N.; Nielsen, S. B.; Otzen, D. E. *FEBS Lett.* **2014**, *588*, 497.
(54) Kong, J.; Yu, S. *Acta Biochim. Biophys. Sin.* **2007**, *39*, 549.
(55) Celej, M. S.; Sarroukh, R.; Goormaghtigh, E.; Fidelio, G. D.; Ruysschaert, J. M.; Raussens, V. *Biochem. J.* **2012**, *443*, 719.
(56) Natalello, A.; Ami, D.; Doglia, S. M. *Intrinsically Disordered Protein Analysis: Methods and Experimental Tools, Methods in Molecular Biology*; Uversky, V. N., Dunker, A. K., Eds.; Springer: New York, 2012; Vol. *1*, pp 229−244
(57) van Rooijen, B. D.; Claessens, M. M.; Subramaniam, V. *Biochim. Biophys. Acta* **2009**, *1788*, 1271.
(58) Apetri, M. M.; Maiti, N. C.; Zagorski, M. G.; Carey, P. R.; Anderson, V. E. *J. Mol. Biol.* **2006**, *355*, 63.
(59) Bolognesi, B.; Kumita, J. R.; Barros, T. P.; Esbjorner, E. K.; Luheshi, L. M.; Crowther, D. C.; Wilson, M. R.; Dobson, C. M.; Favrin, G.; Yerbury, J. J. *ACS Chem. Biol.* **2010**, *5*, 735.
(60) Glatter, O. *J. Appl. Crystallogr.* **1977**, *10*, 415.
(61) Li, J.; Uversky, V. N.; Fink, A. L. *Neurotoxicology* **2002**, *23*, 553.
(62) Binolfi, A.; Rasia, R. M.; Bertoncini, C. W.; Ceolin, M.; Zweckstetter, M.; Griesinger, C.; Jovin, T. M.; Fernandez, C. O. *J. Am. Chem. Soc.* **2006**, *128*, 9893.
(63) Debye, P. *J. Phys. Colloid Chem.* **1947**, *51*, 18.
(64) Fauvet, B.; Mbefo, M. K.; Fares, M. B.; Desobry, C.; Michael, S.; Ardah, M. T.; Tsika, E.; Coune, P.; Prudent, M.; Lion, N.; Eliezer, D.; Moore, D. J.; Schneider, B.; Aebischer, P.; El-Agnaf, O. M.; Masliah, E.; Lashuel, H. A. *J. Biol. Chem.* **2012**, *287*, 15345.
(65) Pedersen, J. S. *J. Appl. Crystallogr.* **2000**, *33*, 637.
(66) Cohen, S. I. A.; Vendruscolo, M.; Dobson, C. M.; Knowles, T. P. J. *J. Chem. Phys.* **2011**, *135*, 065106.
(67) Knowles, T. P.; Waudby, C. A.; Devlin, G. L.; Cohen, S. I.; Aguzzi, A.; Vendruscolo, M.; Terentjev, E. M.; Welland, M. E.; Dobson, C. M. *Science* **2009**, *326*, 1533.
(68) Buell, A. K.; White, D. A.; Meier, C.; Welland, M. E.; Knowles, T. P.; Dobson, C. M. *J. Phys. Chem. B* **2010**, *114*, 10925.
(69) White, D. A.; Buell, A. K.; Dobson, C. M.; Welland, M. E.; Knowles, T. P. J. *FEBS Lett.* **2009**, *583*, 2587.
(70) Zijlstra, N.; Blum, C.; Segers-Nolten, I. M.; Claessens, M. M.; Subramaniam, V. *Angew. Chem., Int. Ed. Engl.* **2012**, *51*, 8821.
(71) Davidson, W. S.; Jonas, A.; Clayton, D. F.; George, J. M. *J. Biol. Chem.* **1998**, *273*, 9443.
(72) Eliezer, D.; Kutluay, E.; Bussell, R., Jr.; Browne, G. *J. Mol. Biol.* **2001**, *307*, 1061.
(73) Ulmer, T. S.; Bax, A.; Cole, N. B.; Nussbaum, R. L. *J. Biol. Chem.* **2005**, *280*, 9595.
(74) van Rooijen, B. D.; van Leijenhorst-Groener, K. A.; Claessens, M. M.; Subramaniam, V. *J. Mol. Biol.* **2009**, *394*, 826.
(75) Milanesi, L.; Sheynis, T.; Xue, W. F.; Orlova, E. V.; Hellewell, A. L.; Jelinek, R.; Hewitt, E. W.; Radford, S. E.; Saibil, H. R. *Proc. Natl. Acad. Sci. U.S.A.* **2012**, *109*, 20455.
(76) Xue, W. F.; Hellewell, A. L.; Gosal, W. S.; Homans, S. W.; Hewitt, E. W.; Radford, S. E. *J. Biol. Chem.* **2009**, *284*, 34272.
(77) Pieri, L.; Madiona, K.; Bousset, L.; Melki, R. *Biophys. J.* **2012**, *102*, 2894.
(78) Stefani, M.; Dobson, C. M. *J. Mol. Med. (Heidelberg, Ger.)* **2003**, *81*, 678.
(79) Fink, A. L. *Factors affecting the fibrillation of a-synuclein, a natively unfolded protein*; Springer: New York, 2007.
(80) Sluzky, V.; Tamada, J. A.; Klibanov, A. M.; Langer, R. *Proc. Natl. Acad. Sci. U.S.A.* **1991**, *88*, 9377.
(81) Campioni, S.; Carret, G.; Jordens, S.; Nicoud, L.; Mezzenga, R.; Riek, R. *J. Am. Chem. Soc.* **2014**, *136*, 2866−2875.
(82) Cremades, N.; Cohen, S. I.; Deas, E.; Abramov, A. Y.; Chen, A. Y.; Orte, A.; Sandal, M.; Clarke, R. W.; Dunne, P.; Aprile, F. A.; Bertoncini, C. W.; Wood, N. W.; Knowles, T. P.; Dobson, C. M.; Klenerman, D. *Cell* **2012**, *149*, 1048.